

yielded when the displacement was small, at this phase, original large compressive stiffness can prevent excessive vertical deformation of 3DIB under accidental vertical load. Along with the increase of vertical loading, the combined disc springs mainly keep linear and elastic but the rhombic steel plate damper yielded with small yield stiffness, close to compressive stiffness of the 3DIB without RADAS. Comparing the compressive behavior of the bearing with and without RADAS, it is concluded that the energy dissipation capacity was essentially limited without RADAS damper, only depended to the friction between each piece of disc spring. The rhombic steel plate damper can provide outstanding energy dissipation capacity to accomplish the purpose of vertical isolation and energy dissipation, which adequately explained the feasibility and effectiveness of the vertical isolation system composed of rhombic steel plate damper and combined disc springs.

Shear performance test of 3DIB was performed by four-bar linkage loading system with experiment device of German SCHENCK electrohydraulic servo loading device, hydraulic pressure lifting jack was employed as vertical loading system. Shear displacement and force of the full-scale 3DIB was measured, and relative deformation between upper and medium joint plate was also recorded at the same time to observe the lateral deformation of the upper part for vertical isolation system of 3DIB and examine that whether the vertical isolation system had enough lateral stiffness or not. Constant vertical compression force was 500kN, the maximum cyclic displacement was 5mm at the first level, the shear displacement increased progressively with 10mm every level up to 60mm, every level contained 3 cycles. Pseudo-static test results revealed that relative deformation of the vertical isolation system was very small under constant vertical pressure and hysteretic shear loading. The shear hysteretic behavior of the 3DIB was shown in Figure 4, it is revealed that a rigid initial stiffness was exhibited by the 3DIB i.e. lead rubber bearing to avoid excessive horizontal shear displacement under minor or medium earthquakes, but shear stiffness evidently decrease when the lead rubber bearing yielded to extend isolation period. On the other hand, the hysteretic circle formed in the pseudo-static test was plentiful which showed the favorable horizontal energy dissipation capacity of the 3DIB. The horizontal pre-yield stiffness of 13.33kN/mm, yield displacement of 3.1mm, yield strength of 41.4kN, yield stiffness of 847kN/m and equivalent stiffness of 1310kN/m of 3DIB was calculated separately according to the hysteretic curve acquired by pseudo-static test. The horizontal pre-yield stiffness of 777.2kN/m and yield strength of 37.2kN of the 3D isolation calculated by theoretical bilinear model was close to measured results, with deviation of 8.2% and 10.1% separately as a result of the variation of material property of rubber and lead material.

CASE STUDY OF A SIMPLIFIED 3D ISOLATED BRIDGE

A three-span girder bridge model as prototype was adopted according to “standard Design Drawings JT/GQB008-96 and JT/GQB009-96” to verify the effectiveness of the proposed 3DIB, with span of 16m and clear width of $9\text{m}+2\times 1.5\text{m}$. Simplified single pier and lumped mass model was used due to minor span and rigid superstructure, without considering soil-pier interaction. The equivalent elastic modulus and density of the bridge was 31.85GPa and 2600kg/m^3 ,

and the proposed 3DIB was installed on the top of the pier. Parameters of the 3DIB measured in pseudo-static test were applied in this analysis. Numerical simulation model was established according to aforesaid parameters and the simplified bilinear model was used for horizontal shear element of 3DIB. Horizontal and vertical component of El Centro record was adopted in time history analysis, with horizontal PGA of 0.31g and vertical PGA of 0.221g.

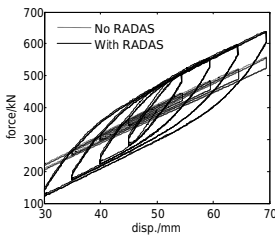


Figure 3. Compressive behavior of the 3DIB.

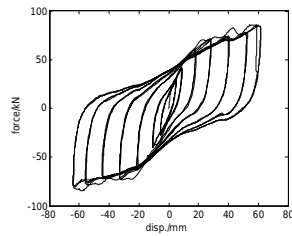


Figure 4. Shear behavior of the 3DIB.

From the horizontal time history analysis of isolated or un-isolated bridge, horizontal displacement and acceleration and moment at the bottom of pier were examined to compare the effectiveness of the isolation bearing. The horizontal displacement of superstructure increased from 21.7mm to 45.9mm, but acceleration decreased from 7.63m/s^2 to 3.69m/s^2 , with a reduction of 51.6%. Moment response at the bottom of pier under horizontal component of El Centro record was shown in Figure 5 and the shear force-displacement of 3DIB i.e. LRB was shown in Figure 6. It is revealed that the maximum moment notably decreased from 2690kN.m to 587kN.m, with reduction of 78.2%, preventing the prematurely serious damage of plastic joint of the pier, excellent energy dissipation capacity was displayed from shear behavior of the bearing, with maximum shear deformation of 43mm, close to 100% of shear deformation of LRB, i.e.50mm, in accordance with expectant design deformation.

Vertical isolation effect is determined by vertical compression stiffness of combined disc spring and stiffness and damping property of rhombic steel plate damper. The combined disc spring with stiffness of 8.12kN/mm and rhombic steel plate with thick of 20mm, width of 100mm and length of 150mm were applied for the adopted model in this case study. Time history analysis was performed on numerical model under vertical component of El Centro record, vertical displacement, acceleration of the upper lumped mass and axial force at the top of pier were examined. The axial force time history before and after seismic isolation were shown in Figure 7, the vertical hysteretic behavior of RADAS damper and 3DIB was shown in Figure 8. It is concluded that the maximum axial force at the top of the pier decreased distinctly, attenuating compression force due to vertical earthquake motions. The variation of compression axial force is from -69.6t to -46.3t before isolation, but it is from -64.6t to -50.0t after isolation. The rhombic steel plate damper

can provide favorable supplementary energy dissipation capacity and greater adding initial stiffness; this is a feasible method for vertical isolation.

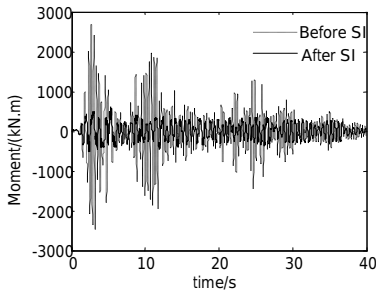


Figure 5. Moment at the bottom of pier.

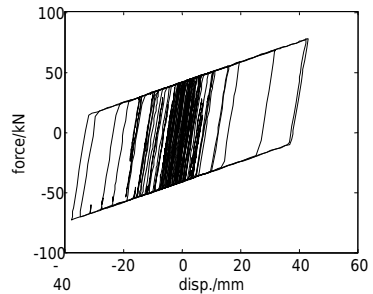


Figure 6. Horizontal hysteretic behavior of 3DIB.

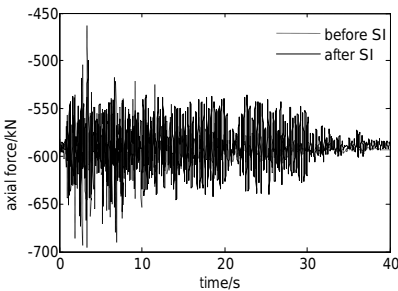


Figure 7. Axial force at the top of pier.

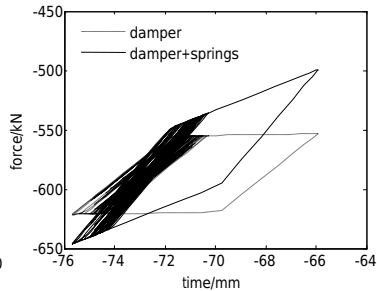


Figure 8. Vertical force-displacement hysteretic curve of RADAS damper and 3DIB.

CONCLUSIONS AND RECOMMENDATIONS

A novel 3D isolation bearing for bridges was proposed and its horizontal and vertical mechanical performance and isolation effect were verified by pseudo-static test and time history analysis on a numerical simulation simplified model. It is concluded that the proposed 3D isolation bearing has reasonable configuration and explicit force transmission mechanism, appropriate horizontal and vertical stiffness and damping property can be achieved by reasonable design, with favorable effectiveness and stability. The rhombic steel plate was effective and feasible for vertical isolation system. Substantial theoretical research and experimental test are essentially needed in future research for the development and engineering application of bridges and other structures.

ACKNOWLEDGEMENT

This research was supported by National Natural Science Foundation of China (Grant No.51208015), China Postdoctoral Science Foundation Funded Project (Grant No.2012M510300) and Beijing Postdoctoral Research Foundation (2012ZZ-15), these supports for this research were definitely appreciated.

REFERENCES

- Chang K.C., Ho M.C., Hwang J.S., Chan T.C., Tao C.C., Wang S.J. (2007). "Development and application of seismic isolation and Energy dissipation systems for buildings in Taiwan". *Journal of Architecture*, No.62, Special Issue on Technology, 133-148.
- Kawashima K. (2001). Remarkable design examples of recent application of seismic isolation to new and reconstructed viaducts in Japan. *The 7th International Seminar on Seismic Isolation, Passive Energy Dissipation and Active Control of Vibrations of Structures*, Assisi, Italy, October 2-5.
- Meng Qingli, Lin Dequan, Zhang Minzheng (2007). "Study on three-dimensional isolated system in shaking table test". *Journal of Earthquake Engineering and Engineering Vibration*, 27(3):116-120.
- Morishita Masaki, Inoue Kazuhiko and Fujita Takafumi (2004). "Development of three-dimensional seismic isolation systems for fast reactor application". *Journal of Japan Association for earthquake Engineering*, 4(3)(Special Issue):305-310.
- Nagarajaiah Satish, Sun Xiaohong (2000). "Response of base-isolated USC hospital building in Northridge Earthquake". *Journal of Structural Engineering*, 126(10):1177-1186.
- Papazoglou A.J. Elnashai A.S. (1996). "Analytical and field evidence of the damaging effect of vertical earthquake ground motion". *Earthquake Engineering and Structural Dynamics*, 25:1109-1137.
- Shi Ming-Hsiang, Sung Wen-pei, Go Cheer-germ(2004). "Investigation of newly developed added damping and stiffness device with low yield strength steel". *Journal of Zhejiang University (Science A)*,5(3):326-334.
- Tsai Keh-Chyuan, Chen Huan-Wei, Hong Ching-Ping and Su Yung-Feng (1993). "Design of steel triangular plate energy absorbers for seismic-resistant construction". *Earthquake Spectra*, 9(3):505-528.
- Wang Zifa (2008). "A preliminary report on the Great Wenchuan Earthquake". *Earthquake Engineering and Engineering Vibration*,7(2):225-234.
- Xu Z D, Shi B Q, Wu K Y, et al. (2009). "Vertical shaking table tests on the structure with viscoelastic multi-dimensional earthquake isolation and mitigation devices". *Sci. China Ser E-tech Sci*, 39(10):1709-1715.
- Zhang Yinghui, Liu Huihang, Wang Decheng. (1997). "Handbook of springs", Beijing: *Mechanical Industry Press*, 1997.

Long-Term Condition Assessment of Stay Cables: Application to Nanjing 3rd Yangtze River Bridge

S. L. Li¹, Y. Xu², H. Li³ and W. M. Yan⁴

¹School of Transportation Science and Engineering, Harbin Institute of Technology, P.O. Box 2537, Harbin; PH (451) 8628-3191; FAX(451)8628-2068; email: lishunlong@hit.edu.cn

²School of Civil Engineering, Harbin Institute of Technology, P.O. Box 2537, Harbin; PH (451) 8628-3191; FAX(451)8628-2068; email: xy_hit2008@126.com

³School of Civil Engineering, Harbin Institute of Technology, P.O. Box 2537, Harbin; PH (451) 8628-2013; FAX(451)8628-2013; email:lihui@hit.edu.cn

⁴Beijing Key Lab of Earthquake Engineering and Structural Retrofit, Beijing University of Technology, Beijing, 100 Pingleyuan; PH (010) 6739-2098; FAX(010) 6739-2098; email: yanwm@bjut.edu.cn

ABSTRACT

This paper presents a long-term condition assessment approach of cables under in-service loads collected by SHM system. For the cables of the bridge, the stochastic axial force response can be collected by the SHM system and described by a filtered Poisson process, through which the maximum value distribution of axial forces in its design reference period can be derived using Poisson Process theory. The long-term deterioration process of steel wires in the cables considers simultaneously the uniform and pitting corrosion due to environmental attack and the fatigue propagation induced by cyclic stress. By employing first order reliability method, the reliability of the cables under the monitored responses is further estimated in terms of the safety under the extreme traffic load distribution in the design reference period and the serviceability specified in the design specification. The discussions of the life-cycle condition assessment of the cable stayed bridge provide guidance to the future decision making related to maintenance and replacement.

INTRODUCTION

Stay cables are always a critical and vulnerable type of structural components in a long-span cable stayed bridge in normal operation conditions. The importance of their safety and serviceability has been recognized by highway administrations throughout the world in securing proper functions of cable-stayed bridges. In the past decades, considerable efforts have been devoted to the condition assessment of steel cables. Sih and Tange (2008) studied the fatigue crack growth behavior of cables and steel wires for the Runyang bridge. Xu and Chen (2008) discussed the failure modes and mechanics of deteriorated steel wires. Rusk and Hoppe (2009) developed the new

model for corrosion damaged high strength steel to predict its fatigue life. Toribio and Matos (2009) dealt with the fatigue crack growth in high strength wires in detailed and discussed the crack front progress by means of aspect ratio evolution with relative crack depth. Most of the previous studies concentrated on the deterioration of high strength steel wires from laboratory testing. Very few studies have been reported on the conditions assessment of stay-cables in operation, which is essential information to optimize their inspection and replacement in real bridge maintenance practice.

This paper presents an investigation of the long-term condition assessment of cables based on the installed SHM system. SHM systems collect massive amounts of in situ data enables the identification of traffic loads, cable forces and structural parameters (global and local). The directly measured cable forces acquired by SHM system are employed to estimate the probabilistic model of cable responses. In the second step, the stochastic deterioration process of steel wires under actual situations is simulated using Monte Carlo approach, in which a coupled corrosion fatigue process of steel wires involving uniform corrosion, pitting corrosion and cyclic fatigue is taken into account. In the third step, the time-variant conditions of the cable due to corrosion fatigue is presented, including the ratio of broken wires, the distribution of crack depth, the remaining cross sectional area and resistance of the suspender. Subsequently, the reliability indices of the cable are evaluated in terms of the safety and serviceability criteria.

NANJING NO. 3 YANGTZE RIVER BRIDGE

The Nanjing No. 3 Yangtze River Bridge, as shown in Figure 1, is one of the largest cable-stayed bridges constructed in the mainland of China. It comprises a main span of 648m and two side spans of 63+257 m each. The bridge tower is as high as 215m and consists 4 transverse beams. The tower below the bridge girder is made of pre-stressed concrete and the rest of the tower is made up of steel plates. There are totally 4×21 pairs of cables. Among the cables, the smallest number of 7mm steel wires consist in a cable is 109, while the largest of is 241.



Figure 1. Nanjing No. 3 Yangtze River Bridge.

RELIABILITY ESTIMATION OF DETERIORATED CABLES

The monitored cable forces results indicate that the cable J06 has the maximum stress range and would be identified as the most critical cable presented hereinafter. Figure 2(a) illustrates one-week cable force time history collected by SHM system. Figure 2(b) shows the distribution of the time intervals between cable force peaks that can be modeled by exponential distribution, while Figure 2(c) presents the distribution of the magnitudes of the peak cable forces, where we can observe two distinct local maxima. Therefore, the peak axial forces, x_M , can be modeled by a bimodal distribution—a superposition of two weighted normal distributions:

$$F_{x_M}(x_M) = p_1 \Phi\left(\frac{x_M - \mu_{M1}}{\sigma_{M1}}\right) + p_2 \Phi\left(\frac{x_M - \mu_{M2}}{\sigma_{M2}}\right) \quad (1)$$

where $p_1 + p_2 = 1$, $p_1 > 0$, $p_2 > 0$, $\Phi(\cdot)$ represents the cumulative probability function of standard normal distribution. Both empirical and theoretical distributions are shown in Figures 2(c), and it is seen that the latter ones match the former ones quite well.

Such a stochastic process of cable forces can be described by a Filtered Poisson Process. In order to conduct safety assessment, it is necessary to estimate the extreme value distribution of loading effects in a certain period. For this purpose, the second peak in Figure 2(c) would apparently govern the extreme value distribution. The stochastic process corresponding to the second peak can be treated as an independent Filtered Poisson Process. The maximum value distribution of trainload-induced axial force in a certain period can be estimated by:

$$F_M(x) = \exp\left\{-\lambda p_2 T_s \left[1 - \Phi\left(\frac{x - \mu_{M2}}{\sigma_{M2}}\right)\right]\right\} \quad (2)$$

where $F_M(x)$ is the cumulative distribution function of the extreme value, λ is the parameter of Poisson Process, determined from the time interval distribution ($\lambda=0.0272$ in this section); T_s is the period of interest in unit of second. Figure 2(d) shows the probability density functions of extreme axial force distributions in different service periods, namely 1 week, 1 year and 100 years.

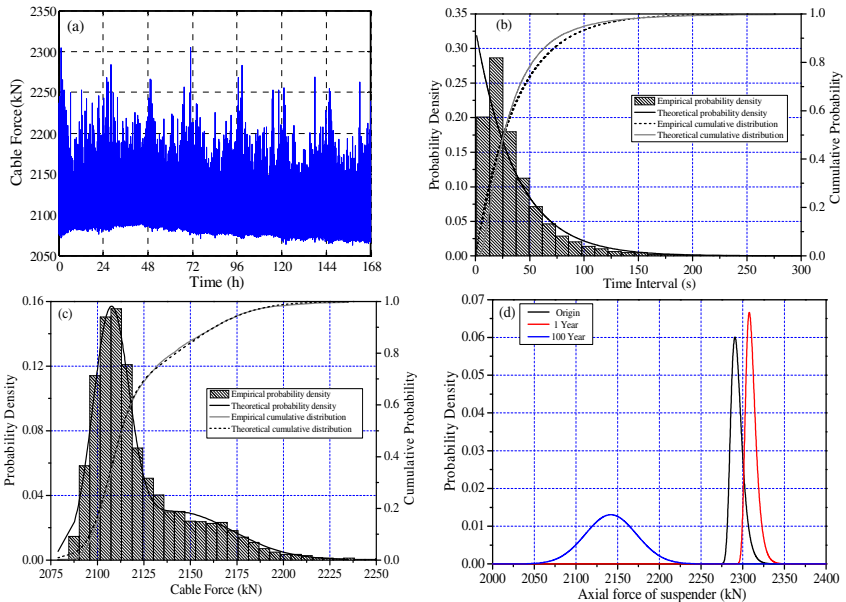


Figure 2. (a) Time history; (b) Distribution of time intervals; (c) Distribution of axial forces; (d) Extreme value distribution in different return periods.

Previous investigations have shown that the uniform corrosion depths of high strength steel wires in a cable are mainly influenced by the corrosion time, the corrosion velocity of galvanized layer and inner steel. The exponential model is one of the widely used empirical models for predicting the atmospheric corrosion depth in steel components

$$v(t) = \psi(t - t_0)^\gamma \tag{3}$$

where $v(t)$ is the corrosion depth at time t ; t_0 represents the time when zinc layer is consumed and steel starts to corrode, ψ and n are model parameters depending on metal type and environmental parameters. The initiation time t_0 can be categorized into four parts according to local environment conditions of steel wires: Part I (1.7 year, wet day and night), Part II (1.7 year, wet at night dry during the day), Part III (6.9 year, soaked in the water day and night) and Part IV (34 year, highly humid day and night). The value of γ is taken as 0.5, and the corrosion rate ψ is proved to follow lognormal distribution whose expected value and variation coefficient are equal to 7.91 $\mu\text{m}/\text{year}$ and 1.14 respectively.

The studies indicated that the penetration of pitting can be treated as a random variable described by the extreme value theory. The ratio of maximum penetration of pitting $a(t)$ to uniform corrosion depth $v(t)$, i.e. $\kappa = a(t)/v(t)$, follows the Extreme Value Type I distribution, and its cumulative distribution function can be expressed as

$$F(\kappa) = \exp\{-\exp[-(\kappa - \beta_0) / \alpha_0]\} \quad (4)$$

where $\alpha_0 = 1.02$ and $\beta_0 = 5.08$ are the distribution parameters estimated from the experimental results for wires with 125 mm length and 8 mm diameter in Hawn (1977). Then the distribution parameters for wires with any given length can be expressed as

$$\beta_\kappa = \beta_0 + 1 / \alpha_0 \ln(A_\kappa / A_0), \alpha_\kappa = \alpha_0 \quad (5)$$

where A_κ represents the surface area of a given high strength wire; A_0 is the surface area of a wire with 125 mm length and 8 mm diameter.

The fatigue crack grows under cyclic stress variation induced by traffic loads. In this study, the axial force response in suspenders is simulated using Monte Carlo simulation based on the Filtered Poisson Process model presented in the last section. The corrosion fatigue crack growth of corrode wires was estimate at the central (deepest) point of the crack front. It is known that for the environmental-assisted fatigue situations, the cracks grow only when the stress intensity factor range ΔK is larger than corrosion fatigue threshold (in this study $2.8 \text{MPa} \cdot \sqrt{m}$). According to the experimental results of Martin and Sanchez (1990), the Paris-Erdogan law can be used for the corrosion fatigue crack growth evaluation.

$$\frac{da}{dN} = C \Delta K^m \quad (6)$$

where da/dN indicates the crack growth rate; m represents the Paris Exponent; $\Delta K = K_{\max} - K_{\min}$ demonstrates the stress intensity factor range, C is crack growth rate. There is a strong correlation between C and m , and their values are highly depending on the environmental aggressiveness. Their results indicated that the coefficient m in the Paris law is around 3 and can be treated as a constant, whereas the crack growth rate of high strength wire, C , has much more randomness and follows the lognormal distribution (its mean value and variation coefficient are equal to 1.069×10^{-11} and 0.095 respectively. It is noted that 3.5 wt% NaCl solution is a common and rational selection in various corrosion test to simulate real corrosion environments of offshore bridges. The stress intensity factor range ΔK at centre point of crack front can be computed by

$$\Delta K = Y \Delta \sigma \sqrt{\pi a} \quad (7)$$

where $\Delta \sigma$ indicates the axial stress range in the cylinder; a represents the depth of crack at time t . The dimensionless stress intensity factor Y for the geometry provided by Astiz (1986).

To evaluate the ultimate load carrying capacity of the cable later on, the time-variant ultimate strength of deteriorated high-strength steel wires is calculated by

$$r^{(l,i)}(t) = \sigma_u^{(l,i)}(t) A_r^{(l,i)}(t) \quad (8)$$

where σ_u and A_r represent, respectively, the ultimate stress and remaining cross section area of steel wires with cracks, and the superscripts illustrate that the deterioration process is dependent on the locations. The ultimate stress σ_u of deteriorated high-strength wires is affected by the existence of unilateral crack, and it can be estimated by fracture mechanics theory, e.g. the PD6493-Lever 3 method generated from the basic theory of J Integral. The corresponding formulations are expressed as follows:

$$\frac{K_I}{K_{IC}} = \left[1 - 0.14 \left(\frac{\sigma_u}{\sigma_y} \right)^2 \right] \cdot \left\{ 0.3 + 0.7 \exp \left[-0.65 \left(\frac{\sigma_u}{\sigma_y} \right)^6 \right] \right\} \quad (9)$$

The time-variant ultimate load-carrying capacity of the suspender cable can be calculated by the synthesis of the remaining strength of the unbroken steel wires at different locations (I = Part I, II, III or IV). With the number of broken wires $k^l(t)$ at time t (obtained in the Monte Carlo simulations) among totally N^l in each category, where the superscripts represent the corresponding location and diameter, the remaining area and strength of unbroken wires can be estimated by

$$A(t) = \sum_i \sum_j A_i^j(t), R(t) = \sum_i \sum_j r^j(t) \quad (10)$$

$t \geq t_0, j = 1, 2, \dots, N^l - k^l$

Figures 3(a) and 3(b) show the statistical results under repeated traffic load actions for steel wires at upper side with a diameter of 7.00 mm (i.e., I = Part II). Figure 3(a) shows the distribution of corrosion fatigue crack depth after 50 year operation time, and Kolmogorov Smirnov (K-S) Hypothesis Testing at significance level of 5% indicates that the distribution does not reject the Generalize Extreme Value Distribution (GEV).

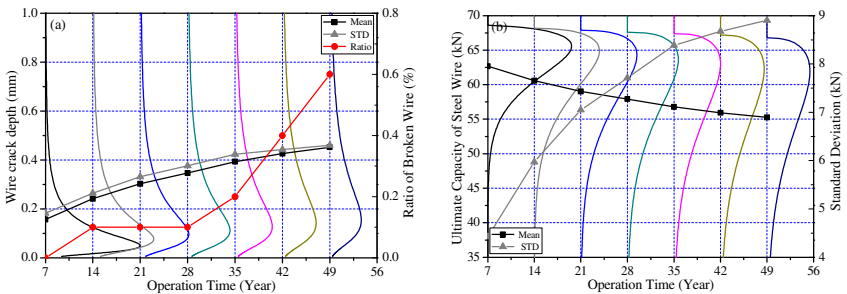


Figure 3. Evolution of wire crack depth and strength and broken wire ratio.

According to China’s Technical Code of Maintenance for City Bridge (J281-2003), the cable in cable-supported bridges should be replaced when the loss of cable’s cross sectional area caused by corrosion exceeds 10%. This criterion is taken as the serviceability limit state of the cable examined in this paper. The safety